

3-26-2025

Galerkin Finite Element Methods Error Estimates Analysis for [1+2] Equations of Integro-Differential on Linear Triangular

Ali Kamil Al-Abadi

Directorate of Education Thi Qar, Ministry of Education, Thi Qar, Iraq and Scientific Research Center, Al-Ayen University, Thi-Qar, Iraq, ali.alabadi@alayen.edu.iq

Shurooq Kamel Abd

College of Computer Science and mathematics, University of Thi-Qar, Nasiriyah, Iraq, shurooqkamel7@gmail.com

Follow this and additional works at: <https://bsj.uobaghdad.edu.iq/home>

How to Cite this Article

Al-Abadi, Ali Kamil and Abd, Shurooq Kamel (2025) "Galerkin Finite Element Methods Error Estimates Analysis for [1+2] Equations of Integro-Differential on Linear Triangular," *Baghdad Science Journal*: Vol. 22: Iss. 3, Article 23.

DOI: <https://doi.org/10.21123/bsj.2024.8848>

This Article is brought to you for free and open access by Baghdad Science Journal. It has been accepted for inclusion in Baghdad Science Journal by an authorized editor of Baghdad Science Journal.



RESEARCH ARTICLE

Galerkin Finite Element Methods Error Estimates Analysis for [1+2] Equations of Integro-Differential on Linear Triangular

Ali Kamil Al-Abadi^{1,2,*}, Shurooq Kamel Abd³

¹ Directorate of Education Thi Qar, Ministry of Education, Thi Qar, Iraq

² Scientific Research Center, Al-Ayen University, Thi-Qar, Iraq

³ College of Computer Science and Mathematics, University of Thi-Qar, Nasiriyah, Iraq

ABSTRACT

In this research, the two-dimensional parabolic integro-differential equation was solved using one of the numerical methods, which is the finite element method (Galerkin) on triangular elements. This method was chosen to make extensive use of finite elements because it has many high-quality numerical properties. The main benefit of finite elements is their ability to solve a wide range of problems in different computational fields in different forms, especially complex ones that cannot be solved by other numerical methods. Given the semi-discrete error estimates for the normal space H^1 , the polynomial linear boundary element space defined in triangles was used to describe space and the inverse Euler method was used to describe time. The discriminant rules used to differentiate the Volterra integral term are also chosen to be compatible with time phase diagrams. In addition, the numerical solutions of the two-dimensional differential integral equation of the equivalent type are compared with the exact solutions, and finally the final results of the solutions are displayed graphically using MATLAB. Finite element Galerkin error analysis was taken into account when using a mesh of triangular elements on the differential equation in two-dimensional space.

Keywords: Backward-Euler, Parabolic integro-differential, Quadrature procedures, Two-dimensional, Volterra integral term

Introduction

The following linear PIDEs are discussed in this article:

$$\frac{\partial p}{\partial t}(x, t) + \mathcal{A}p(x, t) = \int_0^t \mathcal{B}(t, s)p(x, s) ds + f(x, t),$$

$$(x, t) \in \Omega \times (0, T], \quad (1)$$

$$p(x, t) = 0, \quad (x, t) \in \partial\Omega \times [0, T] \quad (2)$$

$$p(x, 0) = u_0(x), \quad x \in \Omega. \quad (3)$$

Here, $\Omega \in \mathbb{R}^2$ be a smooth-bordered bounded domain $\partial\Omega$, as $0 < T < \infty$. Further, $\mathcal{A}p(x, t) = -\Delta p(x, t)$, $\mathcal{B}(t, s)p(x, s) = -\nabla \cdot (\mathcal{B}(t, s)\nabla p(x, s))$, ∇ indicates a spatial gradient and indicates the Laplacian. Suppose that the coefficient matrix $\mathcal{B}(t, s) = \{b_{ij}(\mathbf{x}; t, s)\}$ is 2×2 in $L^\infty(\Omega)^{2 \times 2}$. Taking the initial function as a given $p_0(\mathbf{x})$ belongs to $H^2(\Omega) \cap H_0^1(\Omega)$, the source function $f(\mathbf{x}, t)$ belongs to $L^2(0; T; L^2(\Omega))$ and

$$\max_{\Omega \times \{0 \leq s \leq t \leq T\}} \left| \frac{\partial}{\partial \mathbf{x}} b_{ij}(\mathbf{x}; t, s) \right| < \infty,$$

Ordinary differential equations (ODEs), partial differential equations (PDEs), and integro-differential

Received 4 April 2023; revised 5 March 2024; accepted 7 March 2024.
Available online 26 March 2025

* Corresponding author.

E-mail addresses: ali.alabadi@alayan.edu.iq (A. K. Al-Abadi), shurooqkamel7@gmail.com (S. K. Abd).

<https://doi.org/10.21123/bsj.2024.8848>

2411-7986/© 2025 The Author(s). Published by College of Science for Women, University of Baghdad. This is an open-access article distributed under the terms of the Creative Commons Attribution 4.0 International License, which permits unrestricted use, distribution, and reproduction in any medium, provided the original work is properly cited.

equations (IDEs) can all be solved using the extensive family of numerical and approximation techniques known as finite element methods (FEMs). The FEMs are commonly used because they have many high-quality numerical features. The primary benefit of FEMs is their ability to solve a wide diversity of problems in different computational domains with various shapes. For instance, finite difference methods (FDMs) can solve problems on rectangular and triangular meshes, whereas finite element methods (FEMs) can manage any geometry. The origins of FEMs can be found in 1940s research by Courant and others that focused on applying variational approaches to solve engineering challenges.¹ In the 1950s and 1960s, engineers used FEMs to solve and approximate a wide variety of problems in engineering applications. Beginning in the late 1970s, the FEMs' strong mathematical underpinning was established. A massive number of research papers, books, and monographs about FEMs and their applications have been published in the literature since the 1980s.²

Heat conduction in memory materials,³ compression of poro-viscoelastic media,⁴ nuclear reactor dynamics,⁵ biological epidemic phenomena,⁶ and medication absorption and release⁷ are just a few examples of the many physical situations in which parabolic integro-differential equations (PIDEs) develop. You may find pre-existing and novel solutions to these types of issues in.⁸⁻¹¹

Various techniques, such as spectral methods, spline and collocation, the method of lines, and finite-element techniques,¹²⁻¹⁵ have been devised to numerically solve such equations. Also finite difference,¹⁶ Hybrid¹⁷ and Least-Squares¹⁸ methods. The finite-element method (FEM) stands out as a promising option because it can be applied to non-regular, higher-dimensional domains, and convergence analysis for such problems already exists. In,¹⁹ the authors used FEM to solve parabolic integral differential equations and studied a posteriori error analysis for space-time discretization of the equation in a bounded convex polygonal or polyhedral domain. The piecewise linear finite element spaces are used for space discretization, while the Crank-Nicolson method is used for time discretization. Utilizing nested finite element spaces and the standard energy technique, the proposed method yields an optimal order error estimator for the norm. A standard energy technique coupled with a duality argument is used to derive an error estimate of order for the semi discrete solution when the given initial function is only in time, and²⁰ proves an error estimate of order uniformly in time. A posteriori error estimates were determined by Reddy and Sinha²¹ in 2015 for

the linear parabolic integro-differential equations in a bounded convex polygonal or polyhedral domain using the semi discrete and implicitly completely discrete backward Euler technique. An important use of the Ritz-Volterra reconstruction operator is to provide optimum order a posteriori error estimates in and -norms, using the linear approximation of the Volterra integral component. Additionally, the associated a posteriori error estimates for the reconstruction error of Ritz-Volterra are determined. Shaw and Whiteman investigated a space-time Galerkin finite element discretization of the linear quasistatic compressible viscoelasticity problem described by an elliptic partial differential equation with a Volterra (memory) term in.²² Utilising Galerkin "orthogonality" and the data stability of a related discrete backward problem, they obtained an a priori maximum-energy Galerkin-error estimation.

The article's reminder is structured as follows: In Section Weak formation, the weak formulations are described. In Section Discretizations using Galerkin, the discretization is designed. The numerical scheme of the semi-discrete is discussed in Section Numerical scheme of the semi-discrete. The semi-discrete scheme error estimates are obtained in Section The semi-discrete of error estimates. In Section Scheme of Backward-Euler, the scheme of Backward-Euler is described. In Section Illustration example, a numerical example is given to demonstrate our theoretical analysis. A simple summary of our work is mentioned in the last section.

Everywhere in this article, c will stand for a universally positive constant that is independent, and h the same time, important integral inequality is introduced.

$$\int_0^t \int_0^\tau |\phi|^2 ds d\tau \leq c \int_0^t |\phi|^2 ds, \quad (4)$$

where ϕ is an integrable function in $[0, t]$, $t \in [0, T]$.

Weak formation

Given a Lebesgue measurable set Ω , Lebesgue spaces are denoted by $L^p(\Omega)$, $1 \leq p \leq \infty$. The inner product $\langle \cdot, \cdot \rangle$ is equipped in the space $L^2(\Omega)$ when $p = 2$. Using the conventional notation for Sobolev spaces $W^{m,p}(\omega)$ with $1 \leq p \leq \infty$ for an integer $m > 0$. Sign to $W^{m,2}(\Omega)$ by $H^m(\Omega)$ when $p = 2$. The function space $H_0^1(\Omega)$ is composed of the elements $H^1(\Omega)$ that disappear at $\partial\Omega$. The boundary values in this case this should be interpreted as a trace, and the norm in $L^2 = L^2(\Omega)$ is $\| \cdot \|$, while in $H^m = H^m(\Omega)$ it is $\| \cdot \|_m$.

The differential equation is always rewritten as a variational equation to begin the derivation of a finite element method. This so-called variational formulation is created by multiplying equation Eq. (1) by a test function $v \in H_0^1(\Omega)$ and using Green's formula. The variational problem is what get here: Find $p : [0, T] \rightarrow H_0^1(\Omega)$ where, for all $t \in (0, T]$

$$\int_{\Omega} \frac{\partial p}{\partial t} v dx + a(p, v) = \int_0^t b(t, s; p(s), v) ds + \int_{\Omega} f v dx \quad \forall v \in H_0^1(\Omega), p(\cdot, 0) = p_0. \quad (5)$$

Where

$$a(p, v) = (\nabla p, \nabla v) \quad \forall p, v \in H_0^1(\Omega)$$

and

$$b(t, s; p(s), v) = (B(t, s) \nabla p(s), \nabla v) \quad \forall p(s), v \in H_0^1(\Omega).$$

Discretizations using Galerkin

First, some definitions of projection and its characteristics are given. Let X_h indicates a uniform division of Ω into overlapping triangles K of diameter K_h , so that $\bar{\Omega} = \cup_{K \in T_h} \bar{K}$ every pair of triangles intersects either at a vertex, along an entire edge, or not at all; also, no triangle's vertex is located inside the side of another triangle's interior. Let V_h represent the $H_0^1(\Omega)$ finite dimensional subspaces described by

$$V_h = \{v_h \in H_0^1(\Omega) : v_h|_K \in P_1(K) \quad \forall K \in X_h\}$$

Where P_1 is the space of polynomials of degree at most 1, and V_h satisfy the following inverse property

$$\inf_{v_h \in V_h} \{ \|v - v_h\| + h \|v - v_h\|_1 \} \leq Ch^2 \|v\|^2, \quad \forall v \in H^2 \cap H_0^1, \quad (6)$$

Numerical scheme of the semi-discrete

First, consider the problem of finding semi-discrete $p_h : [0, \infty) \rightarrow V_h$ such that

$$(p_{h,t}, v_h) + a(p_h, v_h) = \int_0^t (b(t, s; p_h(s), v_h) ds) + (f, v_h), \quad \forall v_h \in V_h \quad (7)$$

In,²³ the existence results are covered in detail. Please see²⁴ for outcomes, regularity results, and stability results in²⁵ such problems. Now a numerical chart is displayed. Let $V_h = \text{span} \{\varphi_i\}_{i=1}^N$. Then, any $p_h \in V_h$ have the following expression:

$$p_h = \sum_{i=1}^N p_i \varphi_i,$$

Choosing $v_h = \psi_j, j = 1, 2, \dots, N$ in (6), then Eq. (6) can be expressed in the matrix form as shown below:

$$AP_t + BP = \int_0^t QP(s) ds + F. \quad (8)$$

Where

$$A = (\varphi_i(x), \psi_j(x))_{N \times N},$$

$$B = (\nabla \varphi_i(x), \nabla \psi_j(x))_{N \times N},$$

$$Q = (B(t, s) \nabla \varphi_i(x), \nabla \psi_j(x))_{N \times N},$$

$$F = (f, \psi_j)_{N \times 1},$$

$$P = (p_1, p_2, p_3, \dots, p_N)^T.$$

The semi-discrete of error estimates

In this paragraph, Galerkin finite element method error estimates used in this article are presented. The following projection operator is required to acquire the error estimates: Let $\Pi_h : H_0^1(\Omega) \rightarrow V_h$ is the standard Ritz projection defined by

$$a((p - \Pi_h p), v_h) = 0, \quad \forall v_h \in V_h. \quad (9)$$

The following outcomes are well known to hold²¹

$$\|p - \Pi_h p\| + h \|p - \Pi_h p\|_1 \leq Ch^2 \|p\|_2. \quad (10)$$

Errors were analyzed as follows to obtain prior error estimates:

$$p - p_h = (p - \Pi_h p) + (\Pi_h p - p_h) = \rho + \theta.$$

Applying Eqs. (4) and (6) and supporting projection Eq. (8), the error equation is obtained in θ as

$$(\theta_t, v_h) + a(\theta, v_h) = -(\rho_t, v_h) + \int_0^t (b(t, s; \theta(s), v_h) ds), \quad \forall v_h \in V_h. \quad (11)$$

Now, it is shown how $p - p_h$ error estimates are made.

Theorem: Suppose that $p(t)$ with $p_h(t) \in V_h$ are the solutions of Eq. (6) and Eq. (10). respectively, then for each $T > 0$ there is a constant C_T , therefore

$$\|p - p_h\|_1 \leq Ch \left(\|p\|_2 + h \int_0^T \|p_t\|_2 dt \right)$$

Proof: Estimate ρ of can be obtained from Eq. (9), to estimate θ . We set $v_h = \theta$ in Eq. (10) and obtain

$$(\theta_t, \theta) + a(\theta, \theta) = -(\rho_t, \theta) + \int_0^t (b(t, s; \theta(s), \theta), \theta) ds \tag{12}$$

Using the Schwarz inequality, then Eq. (12) it becomes

$$\frac{1}{2} \frac{d}{dt} \|\theta\|^2 + a(\theta, \theta) = -(\rho_t, \theta) + \int_0^t (b(t, s; \theta(s), \theta), \theta) ds. \tag{13}$$

Taking this equation's integral from 0 to t and ellipticity of a

$$\|\theta(T)\|_1^2 + \int_0^T \|\theta\|_1^2 d\tau \leq C \left(\|\theta(0)\|_1^2 + \int_0^T \|\rho_t\|_1 \cdot \|\theta\|_1 dt + \int_0^T \int_0^t \|\theta(s)\|_1 \|\theta(t)\|_1 ds dt \right) \tag{14}$$

$$2\|\theta(T)\|_1^2 \leq C \left(\|\theta(0)\|_1^2 + \int_0^T \|\rho_t\|_1 \cdot \|\theta\|_1 dt + \int_0^T \int_0^t \|\theta(s)\|_1 \|\theta(t)\|_1 ds dt \right) \tag{15}$$

$$\|\theta(T)\|_1^2 \leq C \left(\|\theta(0)\|_1^2 + \int_0^T \|\rho_t\|_1 \cdot \|\theta\|_1 dt + \int_0^T \int_0^t \|\theta(s)\|_1 \|\theta(t)\|_1 ds dt \right) \tag{16}$$

Noting that $\theta(0) = 0$, these yields

$$\|\theta(T)\|_1^2 \leq C \left(\int_0^T \|\rho_t\|_1 \cdot \|\theta\|_1 dt + \int_0^T \int_0^t \|\theta(s)\|_1 \|\theta(t)\|_1 ds dt \right) \tag{17}$$

Using Eq. (4) with a suitable choice of c for the double integral, getting

$$\|\theta(T)\|_1^2 \leq C \left(\int_0^T \|\rho_t\|_1 \cdot \|\theta\|_1 dt + \int_0^t \|\theta(s)\|_1^2 dt \right) \tag{18}$$

$$\|\theta(T)\|_1 \leq C \left(\int_0^T \|\rho_t\|_1 dt + \int_0^t \|\theta(s)\|_1 dt \right) \tag{19}$$

In order to solve the above equation using Gronwall inequalities,²⁶ one must

$$\|\theta(T)\|_1 \leq C \left(\int_0^T \|\rho_t\|_1 dt \right) \tag{20}$$

From Eq. (10) obtaining

$$\|\theta(T)\|_1 \leq C \left(\int_0^T \|\rho_t\|_1 dt \right) \leq Ch^2 \left(\int_0^T \|p_t\|_2 dt \right) \tag{21}$$

Then, by the triangle inequality

$$\begin{aligned} \|p - p_h\|_1 &= \|p - \Pi_h p + \Pi_h p - p_h\|_1 \\ &\leq \|p - \Pi_h p\|_1 + \|\Pi_h p - p_h\|_1 \\ &\leq \|\rho\|_1 + \|\theta\|_1 \\ &\leq Ch\|p\|_2 + Ch^2 \left(\int_0^T \|p_t\|_2 dt \right) \\ &\leq Ch \left(\|p\|_2 + h \int_0^T \|p_t\|_2 dt \right) \end{aligned} \tag{22}$$

Here, the proof is complete.

Scheme of Backward-Euler

The partition of $[0, T]$ be $0 = t_0 < t_1 < \dots < t_n < \dots < t_N = T$ with $\Delta t = t_n - t_{n-1}$,

$n = 1, 2, \dots, N$ indicate a time grid. Therefore, the fully discrete backward-Euler scheme can be written as follows: find $p^n \in H_0^1(\Omega) \cap \{V = \{v \in C(\bar{\Omega}) : v|_K \in P_1 \forall K \in X_h\}\}$, $n \in [1 : N]$, where

$$\left(\frac{p^n - p^{n-1}}{\Delta t}, v\right) + a(p^n, v) = \delta^n(b(t^n; p, v)) + (f^n, v), \forall v \in V \tag{23}$$

if the left rectangular rule is used to discretize the integral term, or

$$\delta^n(b(t^n; p, v)) = \left\langle \sum_{j=0}^{n-1} \tau_{j+1} B(t_n, t_j) \nabla p(t_j), \nabla v \right\rangle, \tag{24}$$

and, if one applies the right rectangle rule, to have

$$\delta^n(b(t^n; p, v)) = \left\langle \sum_{j=1}^n \tau_j B(t_n, t_j) \nabla p(t_j), \nabla v \right\rangle, \tag{25}$$

and

$$a(p^n, v) = (\nabla p^n, \nabla v). \tag{26}$$

As a result, the discrete problem Eq. (6) is: $p_h^n \in V_h$

$$\left(\frac{p_h^n - p_h^{n-1}}{\Delta t}, v_h\right) + a(p_h^n, v_h) = \delta^n(b(t^n; p_h, v_h)) + (f^n, v_h), \in V_h \tag{27}$$

find $p_h^n = \sum_{j=1}^M p^n(w_j, t_n) \phi_j(x) \in \mathbb{R}^m$ and $v_h = \emptyset_j$ where after simplify, getting

$$(\mathbf{M} + \Delta t \mathbf{A}) p^n = \mathbf{M} p^{n-1} + \Delta t \mathbf{b}^n + (\Delta t)^2 \mathbf{A} (B(t_n, t_0) p^0 + B(t_n, t_{n-1}) p^{n-1}) \tag{28}$$

where \mathbf{M} is a mass matrix, \mathbf{A} is a stiffness matrix and \mathbf{b}^n is a load vector.

Illustration example

The purpose of this section is to provide an illustration to demonstrate the theoretical side discovered in the previous section. Suppose that $\Omega = [-1, 1]^2 \setminus [-1, 0] \times [0, 1]$ is the L-shaped domain and $T = 0.1$. The exact solution $u(x, y, t)$ and fours

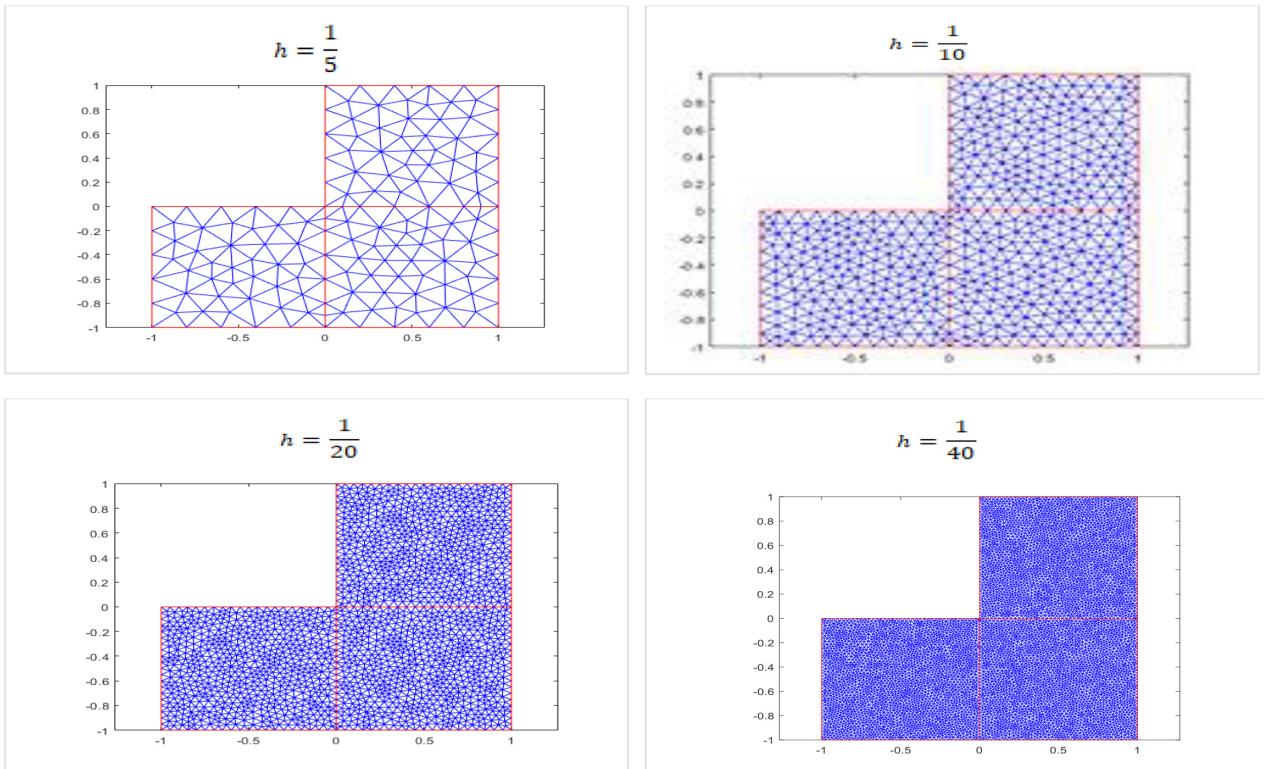


Fig. 1. The levels of grid at $h = \frac{1}{5}, \frac{1}{10}, \frac{1}{20}, \frac{1}{40}$.

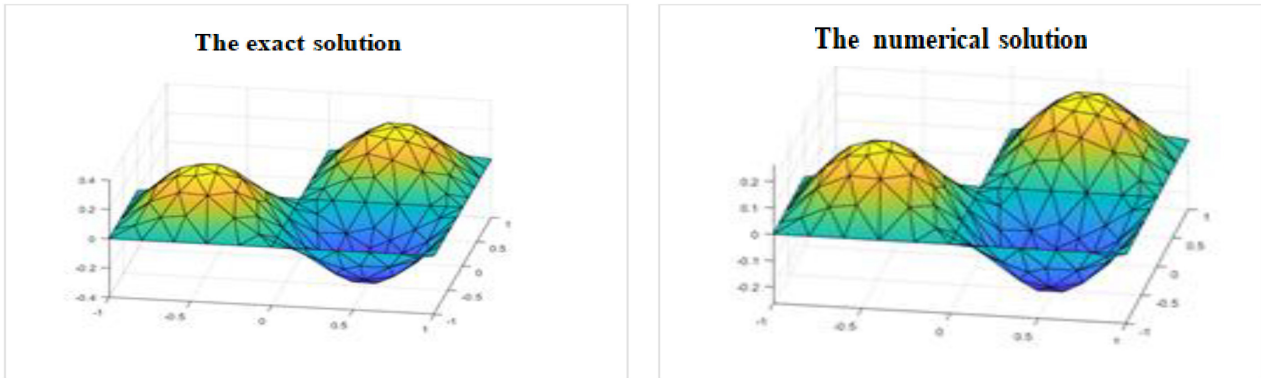


Fig. 2. The exact and numerical solution at $h = \frac{1}{5}$.

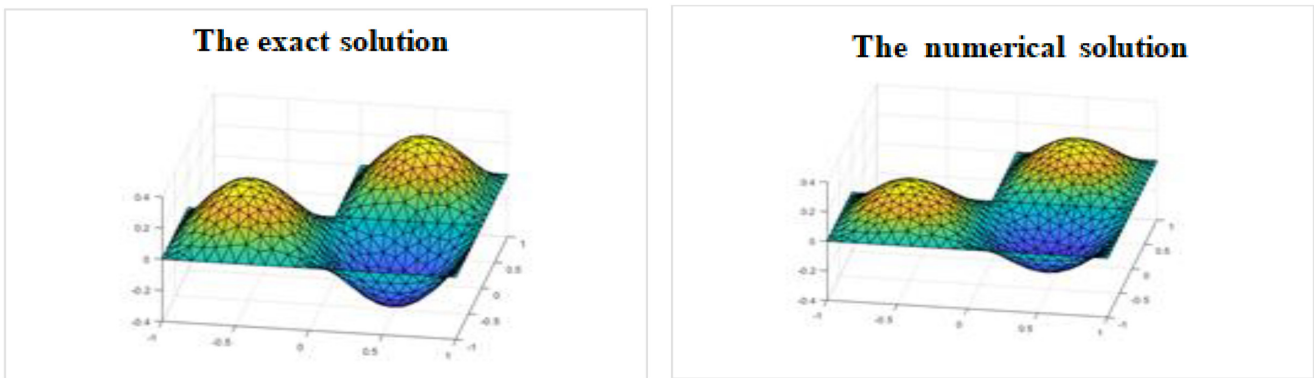


Fig. 3. The exact and numerical solution at $h = \frac{1}{10}$.

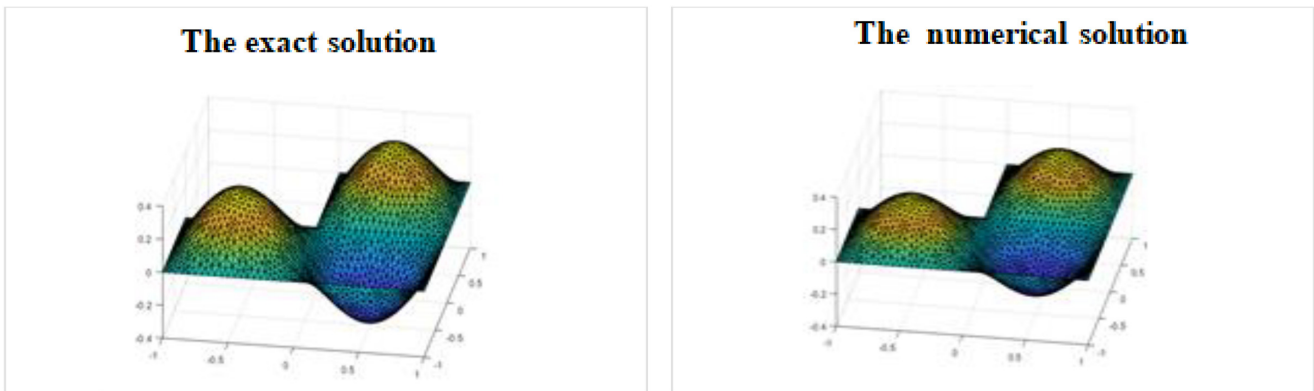


Fig. 4. The exact and numerical solution at $h = \frac{1}{20}$.

function $f(x, t)$ for (1) are selected as

$$u(x, y, t) = e^{-\pi^2 t} \sin(\pi x) \sin(\pi y),$$

$$f(x, y, t) = (1 - 2t) \pi^2 u(x, y, t)$$

and

$$B(t, s) = e^{(-\pi^2(t-s))}$$

This is a kernel that appears in various contexts in several of the older references. The exact numerical solutions and H^1 error of the GFEM Eq. (27) is shown in Table 1 at $\Delta t = .00125$, the convergence rates of the GFEM Eq. (27) are shown in Table 2. Fig. 1 depicts the grid levels at $h = \frac{1}{5}, \frac{1}{10}, \frac{1}{20}, \frac{1}{40}$ and $T = 0, 1$. In Figs. 2 to 4, the exact and numerical solution are shown at $h = \frac{1}{5}, \frac{1}{10}, \frac{1}{20}$, respectively. In Fig. 5, the error of the GFEM Eq. (27)

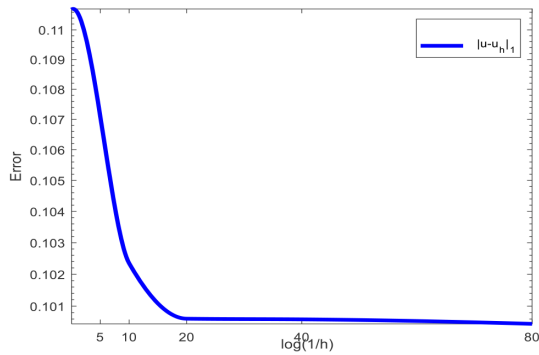


Fig. 5. Error of the GFEM Eq. (27).

Results and discussion

Table 1. The exact, numerical solutions and H^1 error of the GFEM Eq. (27).

h	N	The exact	The numerical	The error
1/5	258	2.6304e-01	3.7013e-01	1.0709e-01
1/10	978	3.7269e-01	2.7139e-01	1.0235e-01
1/20	4086	3.7270e-01	-3.7261e-01	1.0061e-01
1/40	16,406	3.7271e-01	2.7212e-01	1.0059e-01
1/80	66,142	3.7271e-01	2.7226e-01	1.0045e-01

Table 2. Convergence rates of the GFEM Eq. (27).

h	N	Rate
1/5	258	6.5313e-02
1/10	978	2.4737e-02
1/20	4086	2.8682e-04
1/40	16,406	2.0093e-03

Conclusion

In this article, GFEM error analysis was considered when using a mesh of triangular elements on the PIDE in 2D. Utilizing piecewise linear finite element space on triangles and the backward-Euler method for space and time discretization, respectively. The optimal order error constraints are obtained in the H^1 -norm. The associated convergence rates are shown in Table 2. Observations indicate that the convergence rate is roughly equal to 2. As predicted by the theorem, these results demonstrate that the GFEM has optimal order convergence rates for the unknown function. In our next work, how to apply this approach to the analysis of nonlinear integral differential equations will be discussed. This will be done in anticipation of future work.

Acknowledgment

The cooperation of Al-Ayen University in Thi-Qar is appreciated.

Authors' declaration

- Conflicts of Interest: None.
- We hereby confirm that all the Figures and Tables in the manuscript are ours. Furthermore, any Figures and images, that are not ours, have been included with the necessary permission for republication, which is attached to the manuscript.
- No animal studies are present in the manuscript.
- No human studies are present in the manuscript.
- Ethical Clearance: The project was approved by the local ethical committee at University of Thi Qar.

Authors' contribution statement

A. K. A came up with the idea for the article and he also directed the overall endeavour, developed the source code, and produced the paper. S. K. A reviewed the work step by step and made suggestions to improve the scientific and linguistic worth.

References

1. Courant R. Variational methods for the solution of problems equilibrium and vibrations. Bull Amer Math Soc. 1943;49:1–23. <http://dx.doi.org/10.1090/S0002-9904-1943-07818-4>.
2. Zienkiewicz O, Taylor RL, Zhu JZ. The Finite Element Method: Its Basis and Fundamentals. 7th edition. UK: Butterworth-Heinemann. 2013;704 p. <https://doi.org/10.1016/c2009-0-24909-9>.
3. Wang P, Huo J, Wang X-M, Wang B-H. Diffusion and memory effect in a stochastic process and the correspondence to an information propagation in a social system. *Physica A Stat Mech Appl*. 2022;607:128206. <https://doi.org/10.1016/j.physa.2022.128206>.
4. Hosseini-Farid M, Ramzanpour M, McLean J, Ziejewski M, Karami G. A poro-hyper-viscoelastic rate-dependent constitutive modeling for the analysis of brain tissues. *J Mech Behav Biomed Mater*. 2020;102:103475. <https://doi.org/10.1016/j.jmbbm.2019.103475>.
5. Han H, Zhang C. Asymptotical stability of neutral reaction-diffusion equations with PCAS and their finite element methods. *Acta Math Sci*. 2023;43:1865–1880. <https://doi.org/10.1007/s10473-023-0424-9>.
6. Barbeiro S, Ferreira JA. Integro-differential models for percutaneous drug absorption. *Int J Comput Math*. 2007;84(4):451–467. <https://doi.org/10.1080/00207160701210091>.
7. Hussain KH, Hamoud AA, Mohammed NM. Some new uniqueness results for fractional integro-differential equations. *Nonlinear Funct. Anal Appl*. 2019;24(4):827–836.
8. Mohammad M, Trounev A. Fractional nonlinear Volterra-Fredholm integral equations involving Atangana-Baleanu fractional derivative: Framelet applications. *Adv Differ Equ*. 2020;2020:1–15. <https://doi.org/10.1186/s13662-020-03042-9>.
9. Ahmed A. Existence and stability results for fractional volterra-fredholm integro-differential equation with mixed conditions. *Adv Dyn Syst Appl*. 2021;16(1):217–236. <https://doi.org/10.37622/adsa/16.1.2021.217-236>.

10. Sivasankar S, Udhayakumar R. Hilfer fractional neutral stochastic volterra integro-differential inclusions via almost sectorial operators. *Mathematics*. 2022;10(12):1–19. <https://doi.org/10.3390/math10122074>.
11. Gebрил E, El-Azab MS, Sameeh M. Chebyshev collocation method for fractional Newell-Whitehead-Segel equation. *Alex Eng J*. 2024;87:39–46. <https://doi.org/10.1016/j.aej.2023.12.025>.
12. Behera S, Ray SS. An efficient numerical method based on Euler wavelets for solving fractional order pantograph Volterra delay-integro-differential equations. *J Comput Appl Math*. 2022;406:113825. <https://doi.org/10.1016/j.cam.2021.113825>.
13. Xu D. Numerical solution of partial integro-differential equation with a weakly singular kernel based on Sinc methods. *Math Comput Simul*. 2021;190:140–158. <https://doi.org/10.1016/j.matcom.2021.05.014>.
14. Ali I, Yaseen M, Khan S. Addressing volterra partial integro-differential equations through an innovative extended cubic B-Spline collocation technique. *Symmetry*. 2023;15(10):1851. <https://doi.org/10.3390/sym15101851>.
15. Reddy GMM, Sinha RK, Cuminato JA. A posteriori error analysis of the Crank-Nicolson finite element method for parabolic integro-differential equations. *J Sci Comput*. 2019;79:414–441. <https://doi.org/10.1007/s10915-018-0860-1>.
16. Rasheed MA, Kadhim SN. Numerical solutions of two-dimensional vorticity transport equation using crank-nicolson method. *Baghdad Sci J*. 2022;19(2):321–328. <https://doi.org/10.21123/bsj.2022.19.2.0321>.
17. Al-Rozbayani AM, Al-Botani ZM. Solving whitham-broer-kaup-like equations numerically by using hybrid differential transform method and finite differences method. *Baghdad Sci J*. 2022;19(1):64–70. <https://doi.org/10.21123/bsj.2022.19.1.0064>.
18. Noon NJ. Numerical analysis of least-squares group finite element method for coupled Burgers' problem. *Baghdad Sci J*. 2021;18(4(Suppl.)):1521–1535. [https://doi.org/10.21123/bsj.2021.18.4\(Suppl.\).1521](https://doi.org/10.21123/bsj.2021.18.4(Suppl.).1521).
19. Abd SK, Jari RH. Super convergence of finite element approximations for elliptic problem with Neumann boundary condition. *Proceedings of the 1st International Conference on Advanced Research in Pure and Applied Science (ICARPAS 2021): Third Annual Conference of Al-Muthanna University/College of Science, 24–25 March 2021, Al-Samawah, Iraq. AIP Conf. Proc.* 2022. 2398(1):060076. <https://doi.org/10.1063/5.0093736>.
20. Pani AK, Sinha RK. Error estimates for semidiscrete Galerkin approximation to a time dependent parabolic integro-differential equation with nonsmooth data. *Calcolo*. 2000;37:181–205. <https://doi.org/10.1007/s100920070001>.
21. Reddy GMM, Sinha RK. Ritz-Volterra reconstructions and *a posteriori* error analysis of finite element method for parabolic integro-differential equations. *Equations. IMA J. Numer. Anal.* 2015;35(1):341–371. <https://doi.org/10.1093/imanum/drt059>.
22. Shaw S, Whiteman JR. Numerical solution of linear quasistatic hereditary viscoelasticity problems. *SIAM J. Numer. Anal.* 2000;38(1):80–97. <https://doi.org/10.1137/S0036142998337855>.
23. Al-Humedi HA, Al-Abadi AK. Analysis of error estimate for expanded H^1 - Galerkin MFEM of PIDEs with nonlinear memory. *International Conference on Emergency Applications in Material Science and Technology (ICEAMST 2020), 30–31 January 2020, Namakkal, India. AIP Conf Proc.* 2020;2235(1):20010. <http://dx.doi.org/10.1063/5.0007637>.
24. Yanik EG, Fairweather G. Finite element methods for parabolic and hyperbolic partial integro-differential equations. *Nonlinear Anal Theory Methods Appl.* 1988;12(8):785–809. [https://doi.org/10.1016/0362-546X\(88\)90039-9](https://doi.org/10.1016/0362-546X(88)90039-9).
25. Kumar L, Sista SG, Sreenadh K. Finite element analysis of parabolic integro-differential equations of Kirchhoff type. *Math Methods Appl Sci.* 2020;43:9129–9150. <https://doi.org/10.1002/mma.6607>.
26. Barich F. Some Gronwall–Bellman inequalities on time scales and their continuous forms: A survey. *Symmetry*. 2021;13(2):198. <https://doi.org/10.3390/sym13020198>.

تحليل تقديرات الخطأ بطريقة كالركن للعناصر المحدودة للمعادلات التفاضلية التكاملية ذات النمط المكافئ على عنصر مثلث خطي

علي كامل العبادي^{1,2}، شروق كامل عبد³

¹ مديريّة تربية ذي قار، وزارة التربية، ذي قار، العراق.
² وزارة التعليم العالي والبحث العلمي، جامعة العين، ذي قار، العراق
³ كلية علوم الحاسبات والرياضيات، جامعة ذي قار، العراق.

الخلاصة

في هذا البحث تم حل المعادلة التكاملية التفاضلية المكافئة ذات الأبعاد الثنائية باستخدام إحدى الطرق العددية وهي طريقة العناصر المحدودة (جالركين) على العناصر المثلثة. تم اختيار هذه الطريقة للاستفادة على نطاق واسع من العناصر المحدودة لأنها تحتوي على العديد من الخصائص العددية عالية الجودة. الفائدة الأساسية للعناصر المحدودة هي قدرتها على حل مجموعة واسعة من المشاكل في المجالات الحسابية المختلفة بأشكال مختلفة وخصوصاً المعقدة منها والتي لا يمكن حلها بالطرق العددية الأخرى. نظراً لتقديرات الخطأ شبه المنفصلة للمساحة الطبيعية H^1 ، تم استخدام مساحة عنصر الحدود الخطية متعددة الحدود المحددة في المثلثات لوصف المساحة وتم استخدام طريقة أويلر العكسية لوصف الوقت. يتم أيضاً اختيار القواعد التمييزية المستخدمة للتمييز بين مصطلح فولتيرا المتكامل لتكون متوافقة مع مخططات المرحلة الزمنية. بالإضافة إلى ذلك، تتم مقارنة الحلول العددية للمعادلة التكاملية التفاضلية ثنائية الأبعاد من النوع المكافئ مع الحلول الدقيقة، وأخيراً يتم عرض النتائج النهائية للحلول بيانياً باستخدام برنامج MATLAB. وتم أخذ تحليل خطأ جالركين للعنصر المحدود بعين الاعتبار عند استخدام شبكة من العناصر المثلثة على المعادلة التفاضلية في الفضاء ثنائي الأبعاد.

الكلمات المفتاحية: أويلر الخلفي، إجراءات التربيع، المعادلة التكاملية التفاضلية من النوع المكافئ، حد فولتيرا التكاملي، ثنائي الأبعاد،